# Filter Bank Multicarrier Modulation Schemes for Future Mobile Communications

Ronald Nissel, *Student Member, IEEE,* Stefan Schwarz, *Member, IEEE,* and Markus Rupp, *Fellow, IEEE*

***Abstract*—Future wireless systems will be characterized by a large range of possible uses cases. This requires a flexible allocation of the available time-frequency resources, which is difficult in conventional Orthogonal Frequency Division Multiplexing (OFDM). Thus, modifications of OFDM, such as windowing or filtering, become necessary. Alternatively, we can employ a different modulation scheme, such as Filter Bank Multi-Carrier (FBMC). In this paper, we provide a unifying framework, discussion and performance evaluation of FBMC and compare it to OFDM based schemes. Our investigations are not only based on simulations, but are substantiated by real-world testbed measurements and trials, where we show that multiple antennas and channel estimation, two of the main challenges associated with FBMC, can be efficiently dealt with. Additionally, we derive closed-form solutions for the signal-to-interference ratio in doubly-selective channels and show that in many practical cases, one-tap equalizers are sufficient. A downloadable MATLAB code supports reproducibility of our results.**

***Index Terms*—FBMC, OQAM, OFDM, Waveforms, MIMO, Channel Estimation, Time-Frequency Analysis, Measurements**

## I. Introduction

FUTURE mobile systems will be highly heterogeneous and characterized by a large range of possible use cases, ranging from enhanced Mobile BroadBand (eMBB) over enhanced Machine Type Communications (eMTC) to Ultra-Reliable Low latency Communications (URLLC) in vehicular communications [1]–[5]. To efficiently support such diverse use cases, we need a flexible allocation of the available time-frequency resources, as illustrated in Figure 1. There has been a lively discussion both, within the scientific community as well as within standardizations, which modulation format should be used for the next generation of mobile communication systems [6]–[9]. Eventually, 3GPP decided that they will stick to Orthogonal Frequency Division Multiplexing (OFDM) (with some small modifications) for fifth generation (5G) mobile communications [10], [11]. While such decision makes sense in terms of backwards compatibility to fourth generation (4G) wireless systems, it is not the most efficient technique for all possible use cases. Although we do not expect order of magnitude performance gains by switching from OFDM to alternative schemes, it is still important to investigate them because the modulation format lies at the heart of every communication system and determines supported use cases. In this paper, we compare OFDM to Filter Bank Multi-Carrier (FBMC) [12]–[14] which offers much better spectral properties. There exist different variants of FBMC, but we will mainly focus on Offset Quadrature Amplitude Modulation (OQAM) [15] because it provides the highest spectral efficiency. Different names are used to describe OQAM, such as, staggered multitone and cosine-modulated multitone [13], which, however, are essentially all the same [16].

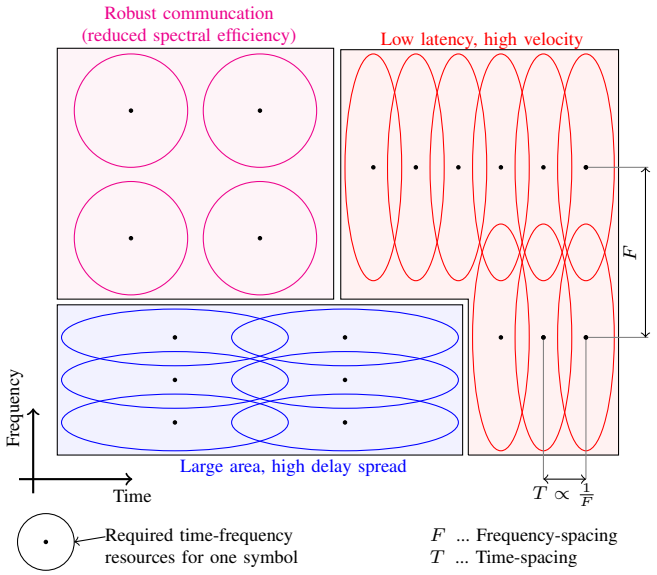


Fig. 1. Future wireless systems should support a large range of possible use cases, which requires a flexible assignment of the time-frequency resources. As indicated in the figure, 5G will employ different subcarrier spacings [11].

In [17], the authors present real-world measurement results for third generation (3G) systems and found that the measured delay spread is much smaller than commonly assumed in mobile communication simulations. They also provide convincing arguments for the lower delay spread, such as, decreasing cell sizes and "spatial filtering" of the environment through beamforming; these arguments will become even more significant in future mobile networks due to increasing network densification, application of massive two-dimensional antenna arrays and the push towards higher carrier frequencies implying larger propagation path losses. A low delay spread was also observed by other measurements [18], [19]. We, hence, identify two key observations for future mobile systems that impact the design of a proper modulation and multiple-access scheme

- Flexible time-frequency allocation to efficiently support

Manuscript was submitted on Dec 16, 2016 and revised on May 1, 2017. The financial support by the Austrian Federal Ministry of Science, Research and Economy, the National Foundation for Research, Technology and Development, and the TU Wien is gratefully acknowledged. R. Nissel, S. Schwarz and M. Rupp are with the Institute of Telecommunications, TU Wien, 1040 Vienna, Austria. R. Nissel and S. Schwarz are also members of the Christian Doppler Laboratory for Dependable Wireless Connectivity for the Society in Motion, TU Wien. (e-mail: {rnissel, sschwarz, mrupp}@nt.tuwien.ac.at

diverse user requirements and channel characteristics.
- Low delay spread, especially in dense heterogeneous networks utilizing Multiple-Input and Multiple-Output (MIMO) beamforming and high carrier frequencies.

These two observations make FBMC a viable choice for future mobile systems due to the following reasons: Firstly, FBMC can be designed to have good localization in both, time and frequency, allowing an efficient allocation of the available time-frequency resources. Secondly, the low delay spread guarantees that simple one-tap equalizers are sufficient to achieve close to optimal performance.

While most papers which investigate FBMC are purely based on simulations, we perform real-world testbed measurements at a carrier frequency of 2.5 GHz (outdoor-to-indoor, 150 m link distance) and 60 GHz (indoor-to-indoor, 5 m link distance). Our measurements support the claim that FBMC is a viable choice for future mobile systems. We follow the measurement methodology presented in [20], [21]. FBMC and OFDM signals are pre-generated off-line in MATLAB and the samples are saved on a hard disk. Then, a Digital-to-Analog-Converter (DAC) together with a radio frequency hardware up-converts the signal to 2.5 GHz, respectively 60 GHz. Different Signal-to-Noise Ratio (SNR) values are obtained by a stepwise attenuator at the transmitter. Furthermore, we relocate the receive antennas within an area of a few wavelengths, resulting in Rayleigh and Rician fading; see for example [22] for a possible fading realization. The receiver itself down-converts the signal and saves the samples on a hard disk. After the measurement, we evaluate the received samples again off-line in MATLAB. Such off-line evaluation represents a cost efficient way of emulating real world transmissions. Pictures of our 2.5 GHz testbed can be found in [23] and of our 60 GHz testbed in [22], [24]. Throughout all of our measurements, simple one-tap equalizers were sufficient in FBMC. Thus, complicated receiver structures, as proposed for example in [25], [26], are not necessary in many scenarios. We also derive a theoretical Signal-to-Interference Ratio (SIR) expression, providing additional analytical insights and allowing FBMC investigations for different channel conditions. Similar work was recently published in [27], [28]. However, the authors of [27] calculate the SIR only for a given channel realization but do not include channel statistics and instead rely on simulations. Authors in [28] utilize the ambiguity function to calculate the SIR. We, on the other hand, employ a simple matrix description and compare the performance to OFDM.

Our contribution can be summarized as follows:

- We validate the applicability of FBMC through real-world testbed measurements and show that many challenges associated with FBMC, such as MIMO and channel estimation, can be efficiently dealt with.
- We show that, from a conceptional point of view, there is little difference in the modulation and demodulation step between FBMC and windowed OFDM. Thus, many hardware components can be reused.
- We propose a novel method to calculate the SIR for doubly-selective channels and show that in many cases, one-tap equalizers are sufficient.
- We show that FBMC allows an efficient co-existence between different use cases within the same band and that it can be efficiently used in low-latency transmissions.
- We provide a detailed tutorial for FBMC, supported by a downloadable MATLAB code[1].

## II. Multicarrier Modulation

In multicarrier systems, information is transmitted over pulses which usually overlap in time and frequency, see Figure 1. Its big advantage is that these pulses commonly occupy only a small bandwidth, so that frequency selective broadband channels transform into multiple, virtually frequency flat, sub-channels (subcarriers) with negligible interference, see Section IV. This enables the application of simple one-tap equalizers, which correspond to maximum likelihood symbol detection in case of Gaussian noise. Furthermore, in many cases, the channel estimation process is simplified, adaptive modulation and coding techniques become applicable, and MIMO can be straightforwardly employed [14]. Mathematically, the transmitted signal $s(t)$ of a multicarrier system in the time domain can be expressed as

$$s(t) = \sum_{k=0}^{K-1} \sum_{l=0}^{L-1} g_{l,k}(t)\, x_{l,k}, \tag{1}$$

where $x_{l,k}$ denotes the transmitted symbol at subcarrier-position $l$ and time-position $k$, and is chosen from a symbol alphabet $\mathcal{A}$, usually a Quadrature Amplitude Modulation (QAM) or a Pulse-Amplitude Modulation (PAM) signal constellation. The transmitted basis pulse $g_{l,k}(t)$ in (1) is defined as

$$g_{l,k}(t) = p(t - kT)\, \mathrm{e}^{\mathrm{j}2\pi\, lF\,(t-kT)}\, \mathrm{e}^{\mathrm{j}\theta_{l,k}}, \tag{2}$$

and is, essentially, a time and frequency shifted version of the prototype filter $p(t)$ with $T$ denoting the time spacing and $F$ the frequency spacing (subcarrier spacing). The choice of the phase shift $\theta_{l,k}$ becomes relevant later in the context of FBMC-OQAM. After transmission over a channel, the received symbols are decoded by projecting the received signal $r(t)$ onto the basis pulses $g_{l,k}(t)$, that is,

$$y_{l,k} = \langle r(t), g_{l,k}(t) \rangle = \int_{-\infty}^{\infty} r(t) g_{l,k}^{*}(t)\, \mathrm{d}t. \tag{3}$$

which corresponds to a matched filter (maximizes the SNR) in an Additive White Gaussian Noise (AWGN) channel. Note that the basis pulses can also be chosen differently at transmitter and receiver [29]. To keep the notation simple, however, we use the same transmit and receive pulse but shall keep in mind that they might be different, especially for Cyclic Prefix (CP)-OFDM and its derivatives.

There exist some fundamental limitations for multicarrier systems, as formulated by the Balian-Low theorem [30], which states that it is mathematically impossible that the following desired properties are all fulfilled at the same time:

[1] **https://www.nt.tuwien.ac.at/downloads/**. All figures can be reproduced (simulations instead of measurements). We also include BER over SNR simulations and time-frequency offset SIR calculations for OFDM, WOLA, UFMC, f-OFDM and FBMC.

TABLE I
COMPARISON OF DIFFERENT MULTICARRIER SCHEMES (FOR AWGN)

| | Maximum Symbol Density | Time-Localization | Frequency-Localization | (Bi)-Orthogonal | Independent Transmit Symbols |
|---|---|---|---|---|---|
| OFDM (no CP) | yes | yes | no | yes | yes |
| Windowed /Filtered OFDM | no | yes | yes | yes | yes |
| FBMC-QAM[1] | no | yes | yes | yes | yes |
| FBMC-OQAM | yes | yes | yes | real only | yes |
| Coded FBMC-OQAM | yes | yes | yes | yes, after de-spreading | no |

[1] There does not exist a unique definition

- Maximum symbol density $TF = 1$
- Time-localization $\sigma_t < \infty$
- Frequency-localization $\sigma_f < \infty$
- Orthogonality, $\langle g_{l_1,k_1}(t), g_{l_2,k_2}(t)\rangle = \delta_{(l_2-l_1),(k_2-k_1)}$,

with $\delta$ denoting the Kronecker delta function. The localization measures $\sigma_t$ and $\sigma_f$ are defined as:

$$\sigma_t = \sqrt{\int_{-\infty}^{\infty} (t-\bar{t})^2 \, |p(t)|^2 \, \mathrm{d}t} \tag{4}$$

$$\sigma_f = \sqrt{\int_{-\infty}^{\infty} (f-\bar{f})^2 \, |P(f)|^2 \, \mathrm{d}f}. \tag{5}$$

where the pulse $p(t)$ is normalized to have unit energy, $\bar{t} = \int_{-\infty}^{\infty} t\,|p(t)|^2\,\mathrm{d}t$ represents the mean time and $\bar{f} = \int_{-\infty}^{\infty} f\,|P(f)|^2\,\mathrm{d}f$ the mean frequency of the pulse. Such localization measures can be interpreted as standard deviation with $|p(t)|^2$ and $|P(f)|^2$ representing the probability density function (pdf), relating the Balian-Low conditions to the Heisenberg uncertainty relationship [31, Chapter 7].

The Balian-Low theorem implies that we have to sacrifice at least one of these desired properties when designing multicarrier waveforms. Table I compares different modulation schemes in the context of the Balian-Low theorem. The different techniques are explained in more detail in the following subsections.

### A. CP-OFDM

CP-OFDM is the most prominent multicarrier scheme and is applied, for example, in Wireless LAN and Long Term Evolution (LTE). CP-OFDM employs rectangular transmit and receive pulses, which greatly reduce the computational complexity. Furthermore, the CP implies that the transmit pulse is slightly longer than the receive pulse, preserving orthogonality in frequency selective channels. The Transmitter (TX) and Receiver (RX) prototype filter are given by

$$p_{\mathrm{TX}}(t) = \begin{cases} \frac{1}{\sqrt{T_0}} & \text{if } -\left(\frac{T_0}{2}+T_{\mathrm{CP}}\right) \le t < \frac{T_0}{2} \\ 0 & \text{otherwise} \end{cases} \tag{6}$$

$$p_{\mathrm{RX}}(t) = \begin{cases} \frac{1}{\sqrt{T_0}} & \text{if } \frac{T_0}{2} \le t < \frac{T_0}{2} \\ 0 & \text{otherwise} \end{cases} \tag{7}$$

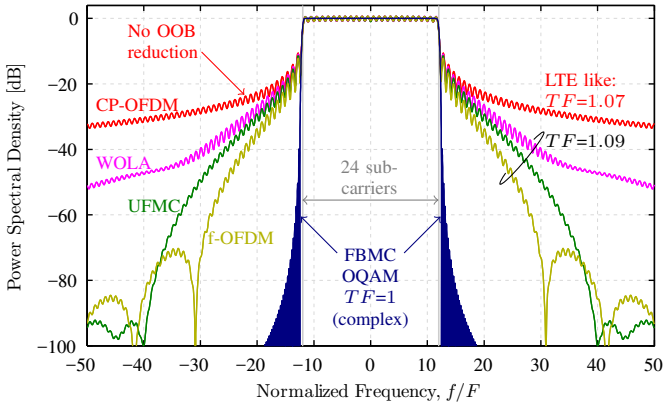


Fig. 2. FBMC has much better spectral properties compared to CP-OFDM. Windowing (WOLA) and filtering (UFMC, f-OFDM) can improve the spectral properties of CP-OFDM. However, FBMC still performs much better and has the additional advantage of maximum symbol density, $TF = 1$ (complex). For FBMC we consider the PHYDYAS prototype filter with $O = 4$.

$$\textbf{(Bi)-Orthogonal}: T = T_0 + T_{\mathrm{CP}};\ F = 1/T_0 \tag{8}$$

$$\textbf{Localization}: \sigma_t = \frac{T_0 + T_{\mathrm{CP}}}{2\sqrt{3}};\ \sigma_f = \infty, \tag{9}$$

where $T_0$ represents a time-scaling parameter and depends on the desired subcarrier spacing (or time-spacing). Unfortunately, the rectangular pulse is not localized in the frequency domain, leading to high Out-Of-Band (OOB) emissions as shown in Figure 2. This is one of the biggest disadvantages of CP-OFDM. Additionally, the CP simplifies equalization in frequency-selective channels but also reduces the spectral efficiency. In an AWGN channel, no CP is needed.

In order to reduce the OOB emissions, 3GPP is currently considering windowing [32] and filtering [4], [33]. The windowed OFDM scheme is called OFDM with Weighted OverLap and Add (WOLA) [32]. At the transmitter, the edges of the rectangular pulse are replaced by a smoother function (windowing) and neighboring WOLA symbols overlap in time. The receiver also applies windowing but the overlapping and add operation is performed within the same WOLA symbol, reducing the inter-band interference. Note that the CP must be long enough to account for both, windowing at the transmitter and at the receiver. For the filtered OFDM scheme, two methods are proposed. Firstly, Universal Filtered Multi-Carrier (UFMC) [33] which applies subband wise filtering based on a Dolph-Chebyshev window. Orthogonality is guaranteed by either Zero Padding (ZP) or a conventional CP. The performance differences between CP and ZP are rather small, so that we will consider only the CP version here to be consistent with the other proposed schemes. The filter parameters are chosen similarly as proposed in [33]. This leads to 12 subcarriers per subband and, if no receive filter is employed, to an orthogonal time-frequency spacing of $TF = 1.07$ (same as in LTE). However, the receive filter is as important as the transmit filter, see Section V. Thus, we also apply subband wise filtering at the receiver. Orthogonality is then guaranteed for a time-frequency spacing of $TF = 1.14$. To improve the spectral efficiency, however, we decrease the time-frequency spacing to $TF = 1.09$ and allow some small

self-interference (≈65 dB). The second filter-based OFDM scheme considered within 3GPP is filtered-OFDM (f-OFDM) [4]. Here, the number of subcarriers for one subband is usually much higher than in UFMC and often includes all subcarriers belonging to a specific use case. The filter itself is based on a sinc pulse (perfect rectangular filter) which is multiplied by a Hann window; other filters are also possible [4]. For a fair comparison, we consider the same time-frequency spacing as in UFMC, that is, $TF = 1.09$ and increase the length of the transmit and receive filters so that self interference is approximately 65 dB. The filters in f-OFDM are usually longer than in UFMC.

As shown in Figure 2, windowing and filtering can reduce the high OOB emissions of CP-OFDM. However, this comes at the price of reduced spectral efficiency, as indicated by the product of $TF$, and lower robustness in frequency selective channels. Furthermore, filtering and windowing still do not provide as low OOB emissions as FBMC (see the next subsection), which can additionally achieve a maximum symbol density of $TF = 1$.

### B. FBMC-QAM

There does not exist a unique definition for FBMC-QAM. Some authors [34] sacrifice frequency localization, making the modulation scheme even worse than OFDM in terms of OOB emissions. Others [35], [36] sacrifice orthogonality in order to have a time-frequency spacing of $TF \approx 1$ and time-frequency localization.

We, on the other hand, consider for FBMC-QAM a time-frequency spacing of $TF = 2$, thus sacrificing spectral efficiency to fulfill all other desired properties; see Table I. Such high time-frequency spacing increases the overall robustness in a doubly-selective channel, see Section IV. However, the main motivation for choosing $TF = 2$ is the straightforward application in FBMC-OQAM, described in the next subsection.

A possible prototype filter for FBMC-QAM is based on Hermite polynomials $H_n(\cdot)$, as proposed in [37]:

$$p(t) = \frac{1}{\sqrt{T_0}} \mathrm{e}^{-2\pi\left(\frac{t}{T_0}\right)^2} \sum_{\substack{i=\{0,4,8,\\ 12,16,20\}}} a_i H_i\left(2\sqrt{\pi}\frac{t}{T_0}\right), \quad (10)$$

for which the coefficients can be found to be [38]

$$\begin{aligned} a_0 &= \ \ 1.412692577 & a_{12} &= -2.2611 \cdot 10^{-9} \\ a_4 &= -3.0145 \cdot 10^{-3} & a_{16} &= -4.4570 \cdot 10^{-15}. \\ a_8 &= -8.8041 \cdot 10^{-6} & a_{20} &= \ \ 1.8633 \cdot 10^{-16} \end{aligned} \quad (11)$$

$$\textbf{Orthogonal}: T = T_0;\ F = 2/T_0 \rightarrow TF = 2 \quad (12)$$

$$\textbf{Localization}: \sigma_t = 0.2015\ T_0;\ \sigma_f = 0.403\ {T_0}^{-1}. \quad (13)$$

Such Hermite pulse has the same shape in time and frequency, allowing us to exploit symmetries. Furthermore, it is based on a Gaussian pulse and therefore has a good joint time-frequency localization $\sigma_t\sigma_f = 1.02 \times 1/4\pi$, almost as good as the bound of $\sigma_t\sigma_f \geq 1/4\pi \approx 0.08$ (attained by the Gaussian pulse), making it relatively robust to doubly-selective channels, see Section IV. Note that no on-line evaluation of the Hermite polynomials is necessary because the sampled version of (10) can be pre-calculated.

Another prominent filter is the so called PHYDYAS prototype filter [12], [39], constructed by:

$$p(t) = \begin{cases} \frac{1+2\sum_{i=1}^{O-1} b_i \cos\left(\frac{2\pi t}{OT_0}\right)}{O\sqrt{T_0}} & \text{if } -\frac{OT_0}{2} < t \leq \frac{OT_0}{2} \\ 0 & \text{otherwise} \end{cases}. \quad (14)$$

The coefficients $b_i$ were calculated in [40] and depend on the overlapping factor $O$ (the interpretation of the overlapping factor will be more clear in Section III). For example, for an overlapping factor of $O = 4$ we have:

$$b_1 = 0.97195983 \quad b_2 = \sqrt{2}/2 \quad b_3 = 0.23514695. \quad (15)$$

$$\textbf{Orthogonal}: T = T_0;\ F = 2/T_0 \rightarrow TF = 2 \quad (16)$$

$$\textbf{Localization}: \sigma_t = 0.2745\ T_0;\ \sigma_f = 0.328\ {T_0}^{-1}. \quad (17)$$

Compared to the Hermite prototype filter, the PHYDYAS filter has better frequency-localization but worse time-localization. The joint time-frequency localization $\sigma_t\sigma_f = 1.13 \times 1/4\pi$ is also worse.

### C. FBMC-OQAM

FBMC-OQAM is related to FBMC-QAM but has the same symbol density as OFDM without CP. To satisfy the Balian-Low theorem, the complex orthogonality condition $\langle g_{l_1,k_1}(t), g_{l_2,k_2}(t)\rangle = \delta_{(l_2-l_1),(k_2-k_1)}$ is replaced by the less strict real orthogonality condition $\Re\{\langle g_{l_1,k_1}(t), g_{l_2,k_2}(t)\rangle\} = \delta_{(l_2-l_1),(k_2-k_1)}$. FBMC-OQAM works, in principle, as follows:

1) Design a prototype filter with $p(t) = p(-t)$ which is orthogonal for a time spacing of $T = T_0$ and a frequency spacing of $F = 2/T_0$, leading to $TF = 2$, see (10), (14).
2) Reduce the (orthogonal) time-frequency spacing by a factor of two each, that is, $T = T_0/2$ and $F = 1/T_0$.
3) The induced interference is shifted to the purely imaginary domain by the phase shift $\theta_{l,k} = \frac{\pi}{2}(l + k)$ in (2).

Although the time-frequency spacing (density) is equal to $TF = 0.5$, we have to keep in mind that only real-valued information symbols can be transmitted in such a way, leading to an equivalent time-frequency spacing of $TF = 1$ for complex symbols. Very often, the real-part of a complex symbol is mapped to the first time-slot and the imaginary-part to the second time-slot, thus the name offset-QAM. However, such self-limitation is not necessary. The main disadvantage of FBMC-OQAM is the loss of complex orthogonality. This implies particularities for some MIMO techniques, such as space-time block codes [41] or maximum likelihood symbol detection [42], as well as for the channel estimation [43].

### D. Coded FBMC-OQAM: Enabling All MIMO Methods

In order to straightforwardly employ all MIMO methods and channel estimation techniques known in OFDM, we have to restore complex orthogonality in FBMC-OQAM. This can be achieved by spreading symbols in time or frequency. Although such spreading is similar to Code Division Multiple Access

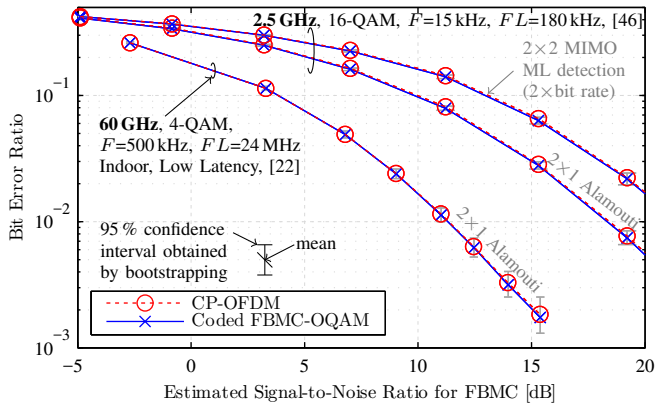


Fig. 3. **Real-world testbed measurements** show that MIMO works in FBMC once we apply coded FBMC-OQAM, that is, spreading symbols in time (or frequency). The spreading process itself has low computational complexity because a fast Walsh-Hadamard transformation can be used. FBMC and OFDM experience both the same BER, but FBMC has lower OOB emissions.

(CDMA), employed in 3G, coded FBMC-OQAM is different in the sense that no rake receiver and no root-raised-cosine filter is necessary. Instead, we employ simple one-tap equalizers which is possible as long as the channel is approximately flat in time (if we spread in time) or in frequency (if we spread in frequency). Because wireless channels are highly underspread [44], such assumption is true in many scenarios. Furthermore, the good time-frequency localization of FBMC allows the efficient separation of different blocks by only one guard symbol and no additional filtering is necessary. Another advantage can be found in the up-link. Conventional FBMC-OQAM requires phase synchronous transmissions ($\theta_{l,k} = \frac{\pi}{2}(l+k)$) which is problematic in the up-link (but not in the down-link) [33]. In coded FBMC, this is no longer an issue because we restore complex orthogonality. The main disadvantage, on the other hand, is the increased sensitivity to doubly-selective channels. This, however, was not an issue in our measurements.

In [42] the authors utilize Fast Fourier Transform (FFT) spreading, while the authors of [41], [45] employ Hadamard spreading. The latter can be implemented by a fast Walsh-Hadamard transform, which reduces the computational complexity and requires no multiplications; we thus prefer it over FFT spreading. In [46], we provide a comprehensive overview of such Hadamard spreading approach and investigate the effects of a time-variant channel.

Figure 3 shows the results of real-world testbed measurements presented in [46] for outdoor-to-indoor transmissions at a carrier frequency of 2.5 GHz and [22] for indoor-to-indoor transmissions at a carrier frequency of 60 GHz. Both, FBMC and OFDM, have the same Bit Error Ratio (BER), validating the spreading approach. However, FBMC has much better spectral properties.

## III. Discrete-Time System Model

The continuous-time representation, described in Section II, provides analytical insights and gives physical meaning to multicarrier systems. However, such representation becomes analytically hard to track in a doubly-selective channel because double integrals have to be solved. Furthermore, in practice, the signal is generated in the discrete-time domain. Thus, we will switch from the continuous-time domain to the discrete-time domain. Additionally, we employ a matrix description, simplifying the system model and allowing us to utilize well-known matrix algebra.

Let us denote the sampling rate by $f_\mathrm{s} = 1/\Delta t = F N_\mathrm{FFT}$, where $N_\mathrm{FFT} \geq L$ represents the size of the FFT; see the next subsection. For the time interval $-OT_0/2 \leq t < OT_0/2 + (K-1)T$ we write the sampled basis pulse $g_{l,k}(t)$, see (2), in a basis pulse vector $\mathbf{g}_{l,k} \in \mathbb{C}^{N\times 1}$, that is,

$$[\mathbf{g}_{l,k}]_i = \sqrt{\Delta t}\; g_{l,k}(t)\big|_{t=i\Delta t - \frac{OT_0}{2}} \quad \text{for} \quad i = 0, 1 \ldots, N-1 \tag{18}$$

$$\text{with} \quad N = (OT_0 + T(K-1))f_\mathrm{s}. \tag{19}$$

By stacking all those basis pulse vectors in a large transmit matrix $\mathbf{G} \in \mathbb{C}^{N\times LK}$ and all data symbols in a large transmit symbol vector $\mathbf{x} \in \mathbb{C}^{LK\times 1}$, according to:

$$\mathbf{G} = \begin{bmatrix} \mathbf{g}_{0,0} & \cdots & \mathbf{g}_{L-1,0} & \mathbf{g}_{0,1} & \cdots & \mathbf{g}_{L-1,K-1} \end{bmatrix}, \tag{20}$$

$$\mathbf{x} = \begin{bmatrix} x_{0,0} & \cdots & x_{L-1,0} & x_{0,1} & \cdots & x_{L-1,K-1} \end{bmatrix}^\mathsf{T}, \tag{21}$$

we can express the sampled transmit signal $\mathbf{s} \in \mathbb{C}^{N\times 1}$ in (1) by:

$$\mathbf{s} = \mathbf{G}\mathbf{x}. \tag{22}$$

Due to linearity, matrix $\mathbf{G}$ can easily be found even if the underlying modulation format is not known in detail. For that, we only have to set all transmitted symbols to zero, except $x_{l,k} = 1$. Vector $\mathbf{s}$ then provides immediately the $l + Lk$-th column vector of $\mathbf{G}$. Repeating this step for each time-frequency position delivers transmit matrix $\mathbf{G}$.

We model multi-path propagation over a doubly-selective channel by a time-variant impulse response $h[m, n]$, where $m$ represents the delay and $n$ the time position. By writing such impulse response in a time-variant convolution matrix $\mathbf{H} \in \mathbb{C}^{N\times N}$, defined as,

$$[\mathbf{H}]_{i,j} = h[i-j, i], \tag{23}$$

we can reformulate the received symbols in (3) by

$$\mathbf{y} = \mathbf{G}^\mathsf{H}\mathbf{r} = \mathbf{G}^\mathsf{H}\mathbf{H}\mathbf{G}\mathbf{x} + \mathbf{n}, \tag{24}$$

whereas $\mathbf{r} \in \mathbb{C}^{N\times 1}$ represents the sampled received signal and $\mathbf{n} \sim \mathcal{CN}(\mathbf{0}, P_\mathrm{n}\,\mathbf{G}^\mathsf{H}\mathbf{G})$ the Gaussian distributed noise, with $P_\mathrm{n}$ the white Gaussian noise power in the time domain. Because wireless channels are highly underspread, the channel induced interference can often be neglected compared to the noise [47]. This means that the off-diagonal elements of $\mathbf{G}^\mathsf{H}\mathbf{H}\mathbf{G}$ are so small, that they are dominated by the noise; see Section IV for more details. Thus, only the diagonal elements of $\mathbf{G}^\mathsf{H}\mathbf{H}\mathbf{G}$ remain, allowing us to factor out the channel according to:

$$\mathbf{y} \approx \mathrm{diag}\{\mathbf{h}\}\,\mathbf{G}^\mathsf{H}\mathbf{G}\,\mathbf{x} + \mathbf{n}, \tag{25}$$

with $\mathbf{h} \in \mathbb{C}^{LK\times 1}$ describing the one-tap channel, that is, the diagonal elements of $\mathbf{G}^\mathsf{H}\mathbf{H}\mathbf{G}$. The operator $\mathrm{diag}\{\cdot\}$ generates a diagonal matrix out of a vector. In OFDM and FBMC-QAM, the orthogonality condition implies that $\mathbf{G}^\mathsf{H}\mathbf{G} = \mathbf{I}_{LK}$

while in FBMC-OQAM we observe only real orthogonality, $\Re\{\mathbf{G}^{\mathsf{H}}\mathbf{G}\} = \mathbf{I}_{LK}$. The imaginary interference in FBMC-OQAM can be canceled by phase equalization of (25) followed by taking the real part. Note that discarding the imaginary interference does not remove any useful information in an AWGN channel. To show that, we utilize a similar approach as for the derivation of the MIMO channel capacity, that is, we employ an eigendecomposition of $\mathbf{G}^{\mathsf{H}}\mathbf{G}$ in (25). We get rid of border effects (which become negligible for a large number of subcarriers and time symbols) by cyclically extending the pulses in time and frequency (which is equivalent to $K \to \infty$ and $L \to \infty$). Then $\mathbf{G}^{\mathsf{H}}\mathbf{G}$ has exactly $LK/2$ non-zero eigenvalues, each having a value of two. This corresponds to the same information rate we can transmit with $LK$ real symbols (the SNR is also the same), so that, by taking the real part, we do not lose any useful information.

The coded-FBMC scheme, see Section II-D, operates on top of an FBMC-OQAM system and can thus be described by

$$\mathbf{x} = \mathbf{C}\,\tilde{\mathbf{x}} \tag{26}$$

$$\tilde{\mathbf{y}} = \mathbf{C}^{\mathsf{H}}\,\mathbf{y}, \tag{27}$$

where $\mathbf{C} \in \mathbb{C}^{LK \times \frac{LK}{2}}$ is the (pre)-coding matrix, $\tilde{\mathbf{x}} \in \mathbb{C}^{\frac{LK}{2}\times 1}$ the transmitted data symbols and $\tilde{\mathbf{y}} \in \mathbb{C}^{\frac{LK}{2}\times 1}$ the received data symbols. To restore orthogonality, the coding matrix has to be chosen such that the zero-forcing condition holds,

$$\mathbf{C}^{\mathsf{H}}\mathbf{G}^{\mathsf{H}}\mathbf{G}\mathbf{C} = \mathbf{I}_{\frac{LK}{2}}, \tag{28}$$

which can be achieved by spreading in time or frequency based on Hadamard matrices. For example, in case of frequency spreading we can express the coding matrix by $\mathbf{C} = \mathbf{I}_K \otimes \mathbf{C}_0$ whereas $\otimes$ represents the Kronecker product. The frequency spreading matrix itself, $\mathbf{C}_0 \in \mathbb{R}^{L\times\frac{L}{2}}$, can be found by taking every second column out of a sequency ordered Walsh-Hadamard matrix $\boldsymbol{\mathcal{H}} \in \mathbb{R}^{L\times L}$, that is, $[\mathbf{C}_0]_{i,j} = [\boldsymbol{\mathcal{H}}]_{i,2j}$. The time spreading approach works in a similar way, but we have to alternate between $[\boldsymbol{\mathcal{H}}]_{i,2j}$ and $[\boldsymbol{\mathcal{H}}]_{i,1+2j}$ for neighboring subcarriers. Of course, the mapping to $\mathbf{C}$ is also different.

For a fair comparison of different modulation schemes, we always consider the same average transmit power $\bar{P}_{\mathrm{S}} = \frac{1}{KT}\int_{-\infty}^{\infty}\mathbb{E}\{|s(t)|^2\}\,\mathrm{d}t$. This leads to a certain per-symbol SNR, defined as $\mathrm{SNR}_{\mathrm{QAM}} = \frac{\mathbb{E}\{|x_{l,k}|^2\}}{P_n}$ and $\mathrm{SNR}_{\mathrm{OQAM}} = \frac{\mathbb{E}\{|x_{l,k}|^2\}}{\frac{1}{2}P_n}$, whereas we assume that the channel has unit power.

One advantage of our matrix notation is the straightforward equalization of the channel in OFDM and FBMC-QAM, for example, by a zero-forcing equalizer $(\mathbf{G}^{\mathsf{H}}\mathbf{H}\mathbf{G})^{-1}$, or a Minimum Mean Squared Error (MMSE) equalizer. In FBMC-OQAM, such direct inversion is not possible because $\mathbf{G}^{\mathsf{H}}\mathbf{H}\mathbf{G}$ has not full rank. Even more problematic is the inherent imaginary interference which influences the performance, so that a straightforward matrix inversion is overall a bad choice. We can avoid some of these problems by stacking real and imaginary part into a supervector, as done in [26], [48] (they do not use our matrix notation). However, all those papers ignore channel estimation and, as we have already elaborated and will further discuss throughout this paper, in almost all practical cases one-tap equalizers are sufficient.

Another advantage of our matrix representation is the straightforward calculation of the expected signal power in time, $\mathbf{P}_{\mathrm{S}} \in \mathbb{R}^{N\times 1}$ :

$$\mathbf{P}_{\mathrm{S}} = \mathrm{diag}\{\mathbb{E}\{\mathbf{s}\mathbf{s}^{\mathsf{H}}\}\} = \mathrm{diag}\{\mathbf{G}\,\mathbf{R}_{\mathbf{x}}\,\mathbf{G}^{\mathsf{H}}\}, \tag{29}$$

whereas $\mathbf{R}_{\mathbf{x}} = \mathbb{E}\{\mathbf{x}\mathbf{x}^{\mathsf{H}}\}$ describes the correlation matrix of the transmit symbols, often an identity matrix. The Power Spectral Density (PSD), $\mathbf{PSD} \in \mathbb{R}^{N\times 1}$, on the other hand, can be calculated by:

$$[\mathbf{PSD}]_j = \sum_{i=0}^{KL-1} |[\mathbf{W}_N\,\mathbf{G}\,\mathbf{U}\,\sqrt{\boldsymbol{\Lambda}}]_{j,i}|^2, \tag{30}$$

where $\mathbf{W}_N$ is the Discrete Fourier Transform (DFT) matrix of size $N$ and $\mathbf{U}$ and $\boldsymbol{\Lambda}$ are obtained by an eigendecomposition of $\mathbf{R}_{\mathbf{x}} = \mathbf{U}\boldsymbol{\Lambda}\mathbf{U}^{\mathsf{H}}$. Again, in many cases $\mathbf{R}_{\mathbf{x}}$ is an identity matrix, leading to $\mathbf{U}\sqrt{\boldsymbol{\Lambda}} = \mathbf{I}_{LK}$. Note that the index $j$ in (30) represents the frequency index with resolution $\Delta f = \frac{f_{\mathrm{s}}}{N}$.

### *IFFT Implementation*

Practical systems must be much more efficient than the simple matrix multiplication in (22). It was shown in [49], for example, that FBMC-OQAM can be efficiently implemented by an Inverse Fast Fourier Transform (IFFT) together with a polyphase network. However, the authors of [49] do not provide an intuitive explanation of their implementation. We therefore investigate an alternative, intuitive, interpretation for such efficient FBMC-OQAM implementation. A similar interpretation was suggested, for example, in [29] for pulse-shaping multicarrier systems, or in [50] for FBMC-OQAM (without theoretical justification). However, most papers still refer to [49] when it comes to an efficient FBMC-OQAM implementation. We therefore feel the need to show that the modulation and demodulation step in FBMC is very simple and actually the same as in windowed OFDM.

To simplify the exposition and without losing generality, we consider only time-position $k = 0$. The main idea is to factor out the prototype filter $p(t)$ from (1):

$$s_0(t) = p(t)\sum_{l=0}^{L-1} \mathrm{e}^{\mathrm{j}2\pi\,lF\,t}\,\mathrm{e}^{\mathrm{j}\theta_{l,0}}\,x_{l,0}. \tag{31}$$

The exponential function in (31) is periodic in $T_0$ due to $F = \frac{1}{T0}$, so that we only have to calculate the exponential summation for the time interval $-T_0/2 \le t < T_0/2$. Furthermore, with the sampling rate $f_{\mathrm{s}} = 1/\Delta t = FN_{\mathrm{FFT}}$, we deduce that the exponential summation corresponds to an $N_{\mathrm{FFT}}$ point inverse DFT. Thus, the sampled version of (31), $\mathbf{s}_0 \in \mathbb{C}^{ON_{\mathrm{FFT}}\times 1}$, can be expressed by ($\mathrm{e}^{\mathrm{j}\theta_{l,0}} = \mathrm{j}^{l+0}$):

$$\mathbf{s}_0 = \mathbf{p} \circ \Bigg( \underbrace{\mathbf{1}_{O\times 1} \otimes \underbrace{\mathbf{W}_{N_{\mathrm{FFT}}}^{\mathsf{H}} \underbrace{\begin{bmatrix} x_{0,0}\,\mathrm{j}^{0+0} \\ \vdots \\ x_{L-1,0}\,\mathrm{j}^{L-1+0} \\ 0 \\ \vdots \end{bmatrix}}_{\text{IFFT}}}_{\text{repeat } O\text{-times}} }_{\text{element-wise multiplication}} \Bigg), \tag{32}$$

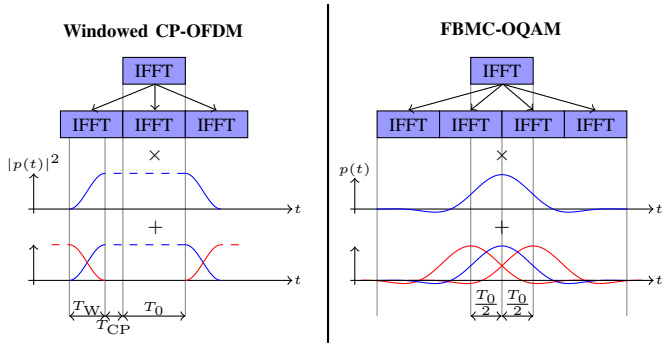


Fig. 4. From a conceptional point of view, the signal generation in windowed OFDM and FBMC-OQAM requires the same basic operations, namely, an IFFT, copying the IFFT output, element wise multiplication with the prototype filter and finally overlapping.

where $\circ$ denotes the element-wise Hadamard product and $\otimes$ the Kronecker product. The sampled prototype filter $\mathbf{p} \in \mathbb{C}^{ON_{\mathrm{FFT}} \times 1}$ in (32) is given by:

$$[\mathbf{p}]_i = \sqrt{\Delta t}\; p(t)\big|_{t=i\Delta t - \frac{OT_0}{2}} \quad \text{for} \quad i = 0, 1 \ldots, ON_{\mathrm{FFT}} - 1. \tag{33}$$

Figure 4 illustrates such low-complexity implementation and compares FBMC-OQAM to windowed OFDM. Both modulation schemes apply the same basic steps, that is, IFFT, repeating and element-wise multiplications. However, windowed OFDM has overall a lower complexity because the element-wise multiplication is limited to a window of size $2T_{\mathrm{W}}$ and time-symbols are further apart, that is, $T = T_{\mathrm{W}} + T_{\mathrm{CP}} + T_0$ in windowed OFDM versus $T = T_0/2$ in FBMC-OQAM. Thus, FBMC needs to apply the IFFT more than two times (exactly two times if $T_{\mathrm{W}} = T_{\mathrm{CP}} = 0$). Of course, the overhead $T_{\mathrm{W}} + T_{\mathrm{CP}}$ in windowed OFDM reduces the throughput. Because the signal generation for both modulation formats is very similar, FBMC-OQAM can utilize the same hardware components as windowed OFDM.

The receiver works in a similar way, but in reversed order, that is, element-wise multiplication, reshaping the received symbol vector to $N_{\mathrm{FFT}} \times O$ followed by a row-wise summation and, finally, an FFT. Note that the same operations are also required in WOLA. In contrast to FBMC, however, the transmit and receive prototype filters are different in WOLA.

## IV. Signal-to-Interference Ratio

So far, we argued that the channel induced interference can be neglected in FBMC systems. This is indeed true for all of our measurements conducted so far. In this section, we will formally derive an analytical SIR expression. Similar to our measurements, we also conclude that the interference can be neglected in many cases, especially if we consider an optimal subcarrier spacing, as also investigated in [28].

### A. QAM

The SIR in case of a QAM transmission can be straightforwardly calculated by employing our matrix notation. We set the noise to zero and evaluate only one received symbol, at subcarrier position $l$ and time-position $k$, so that (24) transforms to:

$$y_{l,k} = \mathbf{g}_{l,k}^{\mathsf{H}}\, \mathbf{H}\, \mathbf{G}\, \mathbf{x} = \Big( (\mathbf{G}\,\mathbf{x})^{\mathsf{T}} \otimes \mathbf{g}_{l,k}^{\mathsf{H}} \Big)\, \mathrm{vec}\{\mathbf{H}\}, \tag{34}$$

where we employ the vectorization operator $\mathrm{vec}\{\cdot\}$ to simplify statistical investigations. The SIR follows directly from (34) and can be expressed as (uncorrelated data symbols):

$$\mathrm{SIR}_i^{\mathrm{QAM}} = \frac{[\mathbf{\Gamma}]_{i,i}}{\mathrm{tr}\{\mathbf{\Gamma}\} - [\mathbf{\Gamma}]_{i,i}} \tag{35}$$

with matrix $\mathbf{\Gamma} \in \mathbb{C}^{LK \times LK}$ given by

$$\mathbf{\Gamma} = \left( \mathbf{G}^{\mathsf{T}} \otimes \mathbf{g}_{l,k}^{\mathsf{H}} \right) \mathbf{R}_{\mathrm{vec}\{\mathbf{H}\}} \left( \mathbf{G}^{\mathsf{T}} \otimes \mathbf{g}_{l,k}^{\mathsf{H}} \right)^{\mathsf{H}}. \tag{36}$$

The correlation matrix $\mathbf{R}_{\mathrm{vec}\{\mathbf{H}\}} = \mathbb{E}\{\mathrm{vec}\{\mathbf{H}\}\mathrm{vec}\{\mathbf{H}\}^{\mathsf{H}}\}$ depends on the underlying channel model and has a major impact on the SIR. Note that $i = l + Lk$ in (35) represents the $i$-th index of the vectorized symbol; see (21) for the underlying structure.

### B. OQAM

The SIR in OQAM transmissions cannot be calculated as easily as in QAM, because OQAM utilizes phase compensation in combination with taking the real part. This is exactly what we have to do in order to calculate the SIR:

$$\mathbf{\Gamma} = \mathbf{\Omega}\mathbf{\Omega}^{\mathsf{H}}, \tag{37}$$

$$[\tilde{\mathbf{\Omega}}_i]_{u,v} = [\mathbf{\Omega}]_{u,v} \frac{|[\mathbf{\Omega}]_{i,v}|}{[\mathbf{\Omega}]_{i,v}}, \tag{38}$$

$$\tilde{\mathbf{\Gamma}}_i = \Re\{\tilde{\mathbf{\Omega}}_i\}\Re\{\tilde{\mathbf{\Omega}}_i\}^{\mathsf{H}}. \tag{39}$$

We perform a matrix decomposition of (36) according to (37), delivering an auxiliary matrix $\mathbf{\Omega} \in \mathbb{C}^{LK \times LK}$ which is phase compensated based on the $i$-th row of $\mathbf{\Omega}$, see (38). As a final step, we combine the phase equalized auxiliary matrix, see (39), allowing us to express the SIR for OQAM by:

$$\mathrm{SIR}_i^{\mathrm{OQAM}} = \frac{[\tilde{\mathbf{\Gamma}}_i]_{i,i}}{\mathrm{tr}\{\tilde{\mathbf{\Gamma}}_i\} - [\tilde{\mathbf{\Gamma}}_i]_{i,i}} \tag{40}$$

### C. Optimal Subcarrier Spacing

For a fair comparison between different modulation formats and filters, we consider an optimal (in terms of maximizing the SIR) subcarrier spacing. As a rule of thumb, the subcarrier spacing should be chosen so that [13]:

$$\frac{\sigma_t}{\sigma_f} \approx \frac{\tau_{\mathrm{rms}}}{\nu_{\mathrm{rms}}}, \tag{41}$$

where time-localization $\sigma_t$ and frequency-localization $\sigma_f$ is given by (13) for the Hermite pulse and by (17) for the PHYDYAS pulse. Note that $F = \frac{1}{T_0}$ in OQAM and $F = \frac{2}{T_0}$ in QAM. For a Jakes Doppler spectrum, the Root Mean Square (RMS) Doppler spread is given by $\nu_{\mathrm{rms}} = \frac{1}{\sqrt{2}}\nu_{\max}$ whereas the maximum Doppler shift can be expressed by $\nu_{\max} = \frac{v}{c} f_{\mathrm{c}}$ with $v$ the velocity, $c$ the speed of light and $f_{\mathrm{c}}$ the carrier frequency. On the other hand, the RMS delay spread is $\tau_{\mathrm{rms}} = 46\,\mathrm{ns}$ for a Pedestrian A channel model and $\tau_{\mathrm{rms}} = 370\,\mathrm{ns}$ for a Vehicular A channel model [51].

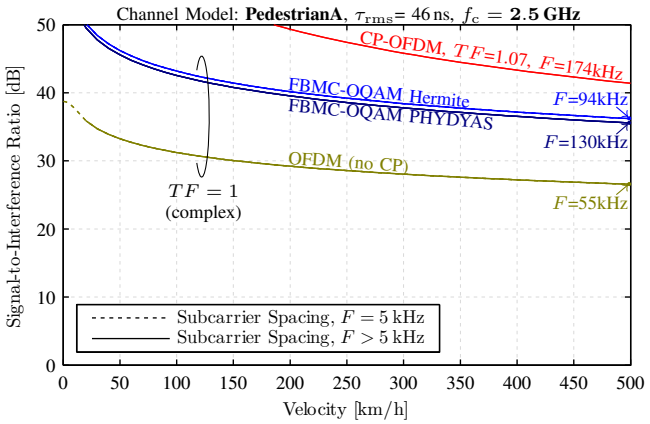


Fig. 5. For a Pedestrian A channel model, the SIR is so high, that the channel induced interference can usually be neglected: it is dominated by the noise.

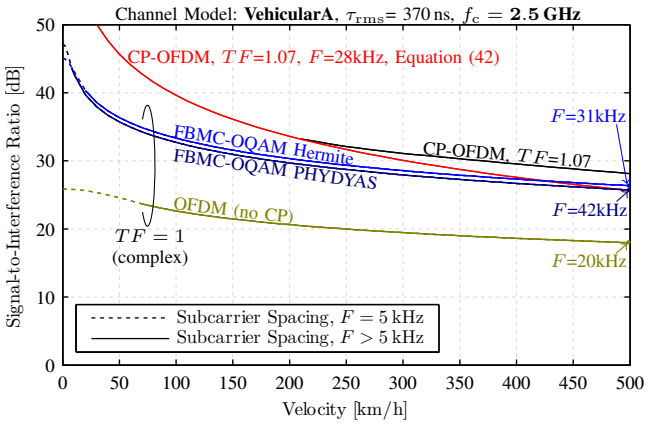


Fig. 6. As in Figure 5, the interference can often be neglected, but now OFDM ($TF = 1.07$) and FBMC have a similar performance for high velocities.

Note that (41) represents only an approximation. The exact relation can be calculated, as for example done in [52] for the Gaussian pulse, and depends on the underlying channel model and prototype filter. However, for our simulation parameters, the differences between the optimal SIR (exhaustive search) and the SIR obtained by applying the rule in (41) is less than 0.1 dB for FBMC-OQAM and less than 1 dB for FBMC-QAM.

As a reference, we also consider an optimal subcarrier spacing in OFDM. The rule in (41), however, cannot be applied because the underlying rectangular pulse is not localized in frequency. Instead, we assume, for a fixed CP overhead of $\kappa = \frac{T_{\text{CP}}}{T_0} = T_{\text{CP}}F = TF - 1$, that the subcarrier spacing is chosen as high as possible while satisfying the condition of no Inter Symbol Interference (ISI), $T_{\text{CP}} = \tau_{\max}$, so that the optimal subcarrier spacing for OFDM transforms to $F = \frac{\kappa}{\tau_{\max}}$. For a Jakes Doppler spectrum, the SIR can be expressed by a generalized hypergeometric function ${}_1F_2(\cdot)$ [53]:

$$\text{SIR}^{\text{OFDM}}_{\text{opt.,noISI}} = \frac{{}_1F_2\left(\frac{1}{2};\frac{3}{2},2;-\left(\pi\frac{\nu_{\max}\tau_{\max}}{TF-1}\right)^2\right)}{1-{}_1F_2\left(\frac{1}{2};\frac{3}{2},2;-\left(\pi\frac{\nu_{\max}\tau_{\max}}{TF-1}\right)^2\right)}, \quad (42)$$

For example, in LTE we have $\kappa = \frac{1}{14} \rightarrow TF = 1.07$. Besides the theoretical expression in (42), we also find the optimal subcarrier spacing through exhaustive search.

Figure 5 shows the SIR over velocity for a Pedestrian A channel model. FBMC is approximately 10 dB better than OFDM without CP. Furthermore, the Hermite filter performs better than the PHYDYAS filter, but only by approximately 0.7 dB. CP-OFDM performs best but also has a lower symbol density ($TF = 1.07$). Overall, the SIR is so high, that noise and other interference sources usually dominate the channel induced interference. Also, the limited symbol alphabet decreases the usefulness of high SNR values, see Section VI-B.

Figure 6 shows similar results as in Figure 5 but for a Vehicular A channel model. The SIR performance is worse than for Pedestrian A but still reasonably high. The SIR for CP-OFDM comes close to FBMC for high velocities, so that CP-OFDM with $TF = 1.07$ no longer provides a much higher SIR compared to FBMC. Note that we assume that the subcarrier spacing is lower bounded by $F \geq 5$ kHz in order to account for latency constraints, computational efficiency and real-world hardware effects. Figure 6 also shows that, in contrast to Figure 5, (42) is no longer optimal for velocities higher than 200 km/h because the optimal subcarrier spacing obtained through exhaustive search leads to a higher SIR by allowing some small ISI (black line).

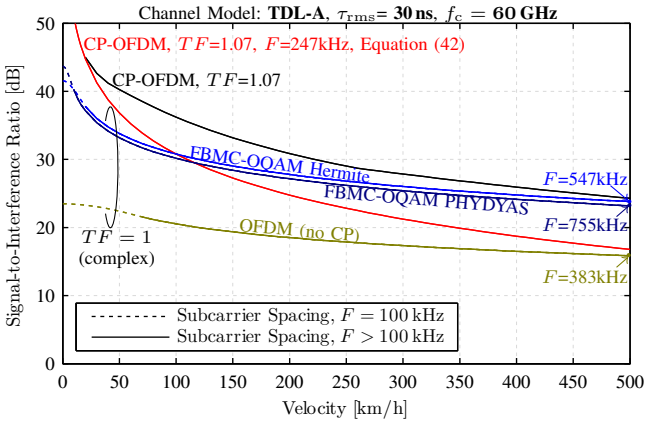


Fig. 7. Even at a carrier frequency of 60 GHz, one tap equalizers are often sufficient, especially if the RMS delay spread is relatively low.

Let us now consider a carrier frequency of 60 GHz. Here, we employ the new Tapped Delay Line (TDL) model proposed by 3GPP [54, Section 7.7.3]. In contrast to Pedestrian A and Vehicular A, the delay taps are no longer fixed but can be scaled to achieve a desired RMS delay spread. Figure 7 show the SIR in case of a TDL-A channel model and the assumption of an RMS delay spread of 30 ns. Overall, we observe a similar behavior as in Figure 6. In particular, for low velocities we can combat frequency selectivity by decreasing the subcarrier spacing, assumed to be lower bounded by $F \geq 100$ kHz. In contrast to the previous results, (42) no longer performs close to the optimum SIR (exhaustive search) because the TDL-A channel model has a very small delay tap very far out, so that the condition of an ISI free transmission is highly suboptimal. Figure 8 shows the SIR for a TDL-B channel model and an RMS delay spread of 900 ns, thus representing a highly doubly-selective channel. We expect that such extreme

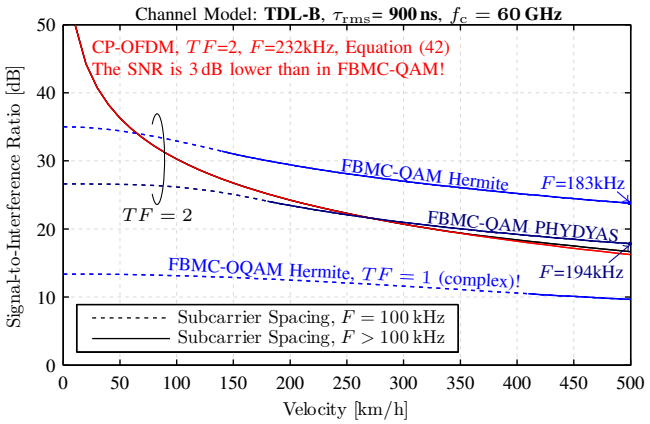


Fig. 8. In the rare case of a highly doubly selective channel, we might need to sacrifice spectral efficiency ($TF = 2$) in order to increase robustness. In such cases, FBMC-QAM even outperforms CP-OFDM (SIR and SNR).

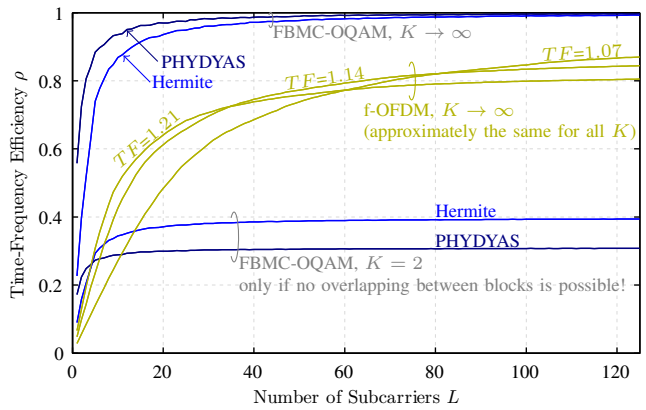


Fig. 9. The time-frequency efficiency depends on the number of subcarriers and the number of time-symbols.

scenarios will rarely happen in reality and a system should therefore not be optimized for such extreme cases, but of course it should be able to cope with it. In FBMC, we can easily combat such harsh channel environments, simply by switching from an FBMC-OQAM transmission to an FBMC-QAM transmission, that is, setting some symbols $x_{l,k}$ to zeros. We thus deliberately sacrifice spectral efficiency, $TF = 2$, in order to gain robustness. It then turns out that FBMC is even better than CP-OFDM. Additionally, the Hermite pulse now outperforms the PHYDYAS pulse because it has a better joint time-frequency localization. In FBMC-OQAM, this effect is somewhat lost due to the time-frequency squeezing. Note that we cannot transmit ISI free CP-OFDM with $TF = 1.07$ because it would require a subcarrier spacing of $F = \frac{1}{14\,\tau_{\max}} = 16\,\text{kHz} < 100\,\text{kHz}$, violating our lower bound.

## V. Possible Use Cases for FBMC

In this section we discuss how FBMC can be utilized to efficiently support different use cases, envisioned for future wireless systems. We start with a definition of the time-frequency efficiency. Then, we assume that two users with two different subcarrier spacings share the same band and calculate the SIR, similar as done in [55]. However, in contrast to [55], we employ a simple matrix notation and compare to OFDM. Finally, we discuss the applicability of FBMC in eMTC and URLLC.

### A. Time-Frequency Efficiency

We define the time-frequency efficiency as

$$\rho = \frac{KL}{(KT + T_{\text{G}})(FL + F_{\text{G}})}, \tag{43}$$

where $T_{\text{G}}$ represents the required guard time and $F_{\text{G}}$ the required guard band. The time-frequency efficiency helps us to answer the question which modulation format utilizes available time-frequency resources best. Note that in the limit of $K \to \infty$ and $L \to \infty$, the time-frequency efficiency depends only on the symbol density $\rho = \frac{1}{TF}$.

Figure 9 compares the time-frequency efficiency of FBMC-OQAM with that of f-OFDM. The guard time $T_{\text{G}}$ is chosen so that 99.99% (= 40 dB) of the transmitted energy, see (29), is within the time interval $KT + T_{\text{G}}$. Similarly, 99.99% of the transmitted energy (utilizing the PSD in (30)) is within the bandwidth $FL + F_{\text{G}}$. Depending on the specific use case, one might want to apply different thresholds. However, the basic statements will stay the same. If only a few time-symbols are used, for example $K = 1$ for f-OFDM and $K = 2$ for FBMC, f-OFDM exhibits better performance than FBMC due to a larger guard time required in FBMC (only if no overlapping between blocks is possible). Approximately $K = 5$ complex time-symbols ($K = 10$ real-symbols) are required to make the time-frequency efficiency of FBMC better than that of f-OFDM, although this depends strongly on the number of subcarriers. Once the number of time-symbols approaches infinity, which is approximately true in many cases because blocks (subframes) can easily overlap, only OOB emissions are relevant and FBMC strongly outperforms f-OFDM. Already $K = 15$ complex time-symbols are sufficient to come close to the limit of $K \to \infty$ for the Hermite pulse (95% threshold); for the PHYDYAS filter it is $K = 30$.

### B. Different Subcarrier Spacings Within The Same Band

Let us now discuss how FBMC can efficiently support different use cases within the same band, as illustrated in Figure 1. For that, we assume two users. User 1 employs a subcarrier spacing of $F_1 = 15\,\text{kHz}$ and user 2 employs $F_2 = 120\,\text{kHz}$. Such different subcarrier spacings will be included in 5G [11] and allow, for example, to deal with different channel conditions, see Section IV. Another reason for different subcarrier spacings are different performance requirements. For example, a high subcarrier spacing allows low latency transmissions whereas a low subcarrier spacing increases the bandwidth efficiency and makes the system more robust to delays.

Our metric of interest here is the SIR. To keep the analysis simple, we ignore the channel (although it could be included similar as in Section IV). The transmitted signal of the first user is characterized by $\mathbf{G}_1$, see (22), and employs $L_1 = 96$ subcarriers with a subcarrier spacing of $F_1 = 15\,\text{kHz}$, leading

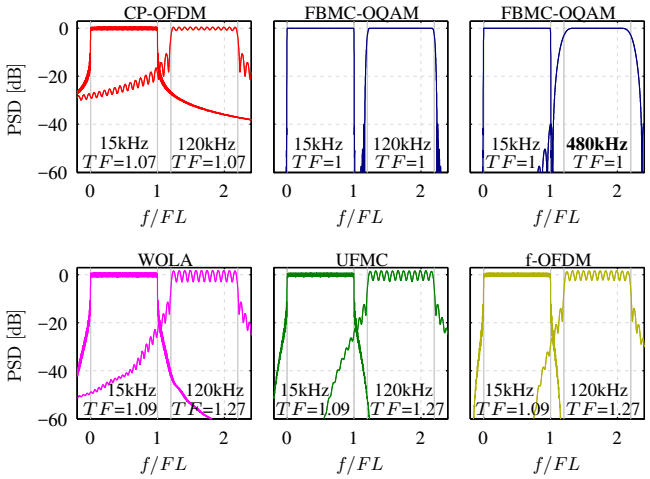


Fig. 10. The PSD in case that two users with different subcarrier spacings ($F_1 = 15\,\text{kHz}$, $F_2 = 120\,\text{kHz}$) share the same band. The transmission bandwidth is the same for both users $F_1 L_1 = F_2 L_2 = 1.44\,\text{MHz}$. In case of FBMC, we also consider a subcarrier spacing of $F_2 = 480\,\text{kHz}$, leading to approximately the same latency as for OFDM with $F_2 = 120\,\text{kHz}$. In this example, the guard band is set to $F_\text{G} = 0.2\,F_1 L_1$.

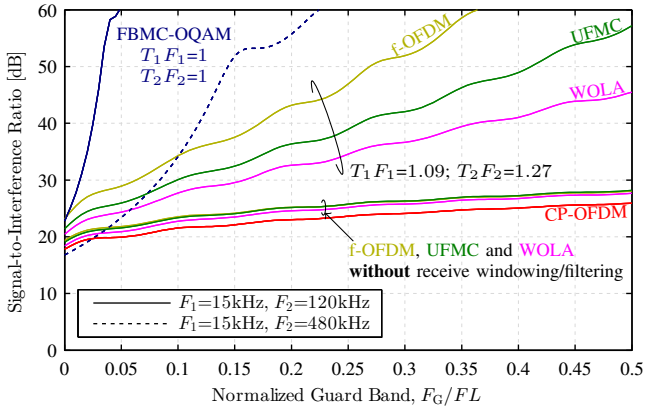


Fig. 11. FBMC has a higher SIR than OFDM, so that the required guard band is much smaller. Compared to the channel induced inference, see Section IV, we often require a much higher SIR due to different receive power levels (not included in (44) to keep the notation simple). Windowed and filtered OFDM only perform well if windowing and filtering is also applied at the receiver.

to a transmission bandwidth of $F_1 L_1 = 1.44\,\text{MHz}$. Similarly, the second user is characterized by $\mathbf{G}_2$, employs $L_2 = 12$ subcarriers with a subcarrier spacing of $F_2 = 120\,\text{kHz}$, leading to the same bandwidth as before, that is, $L_2 F_2 = 1.44\,\text{MHz}$. Additionally, $\mathbf{G}_2$ is shifted in frequency by $F_1 L_1 + F_\text{G}$. Figure 10 shows the PSD, see (30), for both users and a guard band of $F_\text{G} = 0.2\,F_1 L_1$. For WOLA, UFMC and f-OFDM, we assume a time-frequency spacing of $T_1 F_1 = 1.09$ for the first user, same as in Figure 2. For the second user, on the other hand, we assume a time-frequency spacing of $T_2 F_2 = 1.27$ in order to reduce the OOB emissions further. Our proposed matrix notation again simplifies the analytical calculation of the total SIR, defined for FBMC-OQAM as:

$$\text{SIR}_\text{total,2-use-case} = \frac{L_1 K_1 + L_2 K_2}{||\Re\{\mathbf{G}_1^\text{H}\mathbf{G}_2\}||_\text{F}^2 + ||\Re\{\mathbf{G}_2^\text{H}\mathbf{G}_1\}||_\text{F}^2}, \quad (44)$$

where $||\cdot||_\text{F}$ represents the Frobenius norm. To keep the notation in (44) simple, we ignore self interference (≈65 dB) within one use case, that is, the off-diagonal elements of $\mathbf{G}_1^\text{H}\mathbf{G}_1$ and $\mathbf{G}_2^\text{H}\mathbf{G}_2$. In CP-OFDM, WOLA, UFMC and f-OFDM, the $\Re\{\}$ in (44) disappears because we operate in the complex domain. Furthermore, the transmit and receive matrices are different. In (44) we consider the sum interference power but should keep in mind that subcarriers close to the other user experience a higher interference than subcarriers farther away. Furthermore, to keep the notation simple, (44) does not account for different receive power levels caused by different transmit power levels and different path losses. Thus, compared to Section IV, we require a higher SIR to account for those factors. Figure 11 shows how the SIR, see (44), depends on the normalized guard band, whereas we assume $K \gg 1$, so that $T + \frac{T_\text{G}}{K} \approx T$. The higher the guard band, the less interference we observe. As illustrated in Figure 11, receive windowing and filtering are of utmost importance. Without it, there is not much difference between WOLA, UFMC, f-OFDM and conventional CP-OFDM [56].

Additionally, we should keep in mind that, without receive windowing and filtering, the interference from user 1 to user 2 is higher than the interference from user 2 to user 1, which can be deduced from Figure 10. Once we apply windowing and filtering at the receiver, both users experience approximately the same interference power. As shown in Figure 11, WOLA, UFMC and f-OFDM can improve the SIR but the performance is still not as good as in FBMC. Let us assume we require an SIR of 45 dB. Then, f-OFDM needs a guard band of $F_\text{G} = 0.24\,FL$. Thus, the time-frequency efficiency for user 2 becomes $\rho = \frac{1}{1.24 \times 1.27} = 0.64$. In contrast to that, FBMC has a much higher efficiency of $\rho = 0.97$. Therefore, the data rate in FBMC is approximately 50 % higher than in f-OFDM. One reason for the high subcarrier spacing of user 2 ($F_2 = 120\,\text{kHz}$) is to enable low latency transmissions. This implies that, for a fair comparison in terms of latency, we have to increase the subcarrier spacing in FBMC further by a factor of four ($O = 4$), leading to $F = 480\,\text{kHz}$ and thus approximately the same latency as in OFDM. The number of subcarriers in FBMC then decreases from $L = 12$ to only $L = 3$. As shown in Figure 11, a higher subcarrier spacing ($F = 480\,\text{kHz}$) requires a larger guard band ($F_\text{G} = 0.13\,FL$ for a 45 dB SIR threshold), but the time-frequency efficiency ($\rho = 0.88$) is still approximately 40% higher than in f-OFDM. Thus, the statement that FBMC is not suited for low-latency transmissions is not true in general. We only have to increase the subcarrier spacing. Of course, this further increases the sensitivity to time-offsets and delay spreads (but decreases the sensitivity to frequency-offsets and Doppler spreads). Note that the superior spectral properties of FBMC also simplify frequency synchronization [57].

Once we apply a higher bandwidth per user, say 10.08 MHz instead of 1.44 MHz, the possible improvement of FBMC compared to f-OFDM reduces to only 15% (45 dB SIR threshold).

### C. eMTC and URLLC

If the number of subcarriers is high, OFDM has a relatively high spectral efficiency. This will usually be the case in eMBB.

However, other use cases, such as eMTC, might not always employ a high number of subcarriers (per user/machine). FBMC then becomes much more efficient, as already discussed in the previous subsection. If only one subcarrier is active, FBMC can even act as a single carrier scheme with the advantage of a reduced Peak-to-Average Power Ratio (PAPR). The time-frequency efficiency then decreases but is still much higher than in OFDM. If the bandwidth is sufficiently small, we can also employ simple one-tap equalizers and have the additional advantage of a high SNR. Of course, a small bandwidth implies low data rates but many use cases do not require high data rates.

Another important use case is URLLC. We have already shown in the previous subsection that FBMC has a higher spectral efficiency than OFDM in low latency scenarios. We only need a high subcarrier spacing. For example, we were able to transmit a $2\times1$ Alamouti FBMC and OFDM signal (one subframe) within less than $40\,\mu$s [22], thus satisfying the low latency condition [58] (the evaluation was performed off-line to keep hardware costs reasonable low). High reliability can also be achieved in FBMC by switching from an FBMC-OQAM transmission to an FBMC-QAM transmission, thus, deliberately sacrificing spectral efficiency but improving robustness in doubly-selective channels and with respect to time-frequency offsets. Of course, we have to include additional steps, such as diversity (frequency, space), to guarantee high reliability.

## VI. Further Discussions

### A. Channel Estimation

In FBMC-QAM and coded FBMC-OQAM, we can straightforwardly employ all OFDM channel estimation methods known in literature. In FBMC-OQAM, however, this is not possible. The main idea of FBMC-OQAM is to equalize the phase followed by taking the real part in order to get rid of the imaginary interference. This, however, only works once the phase is known, thus only after channel estimation. The channel estimation has to be performed in the complex domain where we observe imaginary interference, so that the estimation process becomes more challenging. Possible solutions for preamble-based channel estimation are discussed in [59]–[62]. However, in a time-variant channel, pilot symbol aided channel estimation is usually preferred over preamble based methods because pilots allow to track the channel. A simple method for pilot aided channel estimation was proposed in [63], where one data symbol per pilot is sacrificed to cancel the imaginary interference at pilot position. Authors in [64] proposed the name auxiliary symbol for such method. The big disadvantage is the high power of the auxiliary symbols, worsening the PAPR and wasting signal power. Subsequently, different methods have been proposed to mitigate these harmful effects [38], [65]–[69]. From all those techniques, we think that the data spreading approach [65] is the most promising method because no energy is wasted, there is no noise enhancement, and the performance is close to OFDM [43]. The idea of [65] is to spread data symbols over several time-frequency positions (close to the pilot symbol) in such a way, that the imaginary interference at the pilot position is canceled. The drawback is a slightly higher computational complexity due to de-spreading at the receiver [38]. This complexity, however, can be reduced by a Fast-Walsh Hadamard transform and by exploiting the limited symbol alphabet (at least at the transmitter). Another way of reducing the complexity is to combine it with the method of [63], as proposed in [70] (the performance becomes slightly worse because now energy is wasted). Note that the spreading method also performs reasonably well in doubly-selective channels [71]. For a more detailed comparison of pilot-symbol aided channel estimation in OQAM we refer to [38], [72].

### B. Performance Metric

In order to compare different modulation schemes, we have to find a meaningful metric. Some authors, such as [65], use the BER over $E_b/N_0$ to compare FBMC with CP-OFDM. However, in our opinion, $E_b/N_0$ has some serious drawbacks. To understand why, let us assume a signal 1, consisting of two OFDM symbols (without CP), and a signal 2, consisting of one OFDM symbol where the CP is as long as the useful symbol duration. Thus, both signals occupy the same time duration. However, the same $E_b/N_0$ implies that there is a 3 dB difference in transmit power between the signals. In our opinion, a meaningful comparison must include the same transmit power. This results in the same receive SNR and thus the same BER (AWGN channel). However, signal 1 has twice the data rate. The idea in $E_b/N_0$ is to account for such different data rates, but a simple power normalization is not a good solution because the symbol power affects the rate only logarithmically. Instead, we should use the achievable rate (capacity) and the throughput. The ergodic capacity [73] for one time-frequency position is:

$$C = \mathbb{E}_h\left\{\log_2\left(1+|h|^2\,\mathrm{SNR}\right)\right\}. \tag{45}$$

Such expression assumes Gaussian inputs which is an unrealistic assumption. The data symbols are usually chosen from a fixed signal constellation which is included in the Bit-Interleaved Coded Modulation (BICM) capacity [74], [75]:

$$C_{\mathrm{B}} = \mathbb{E}_h\left\{\max_{\substack{\mathcal{X}\in\{\mathcal{A}_1,\\ \mathcal{A}_2,\ldots\}}}\left(m-\sum_{i=1}^{m}\mathbb{E}_{b,y|h}\left[\log_2\frac{\sum\limits_{x\in\mathcal{X}}\mathrm{pdf}_h(y|x)}{\sum\limits_{x\in\mathcal{X}_b^i}\mathrm{pdf}_h(y|x)}\right]\right)\right\} \tag{46}$$

where $\mathcal{X}$ is the symbol alphabet and $\mathcal{X}_b^i$ the subset of $\mathcal{X}$ whose label has the bit value $b\in\{0,1\}$ at position $i$. In contrast to [74] we also include an adaptive symbol alphabet $\{\mathcal{A}_1,\mathcal{A}_2,\ldots\}=\{4,16,\ldots\}$-QAM. We could also include channel estimation in our BICM expressions [76], [77], but assuming perfect channel knowledge provides enough insights to get an understanding of the system. The achievable rate is then obtained by $\frac{L}{T}C$ where we account for the bandwidth (number of subcarriers) and the time-spacing. If pilot symbols are included, the achievable rate is accordingly lower.

Figure 12 shows the measured throughput [78] as well as the theoretical bounds discussed so far (for Rayleigh fading). FBMC has a higher throughput than OFDM due to a higher

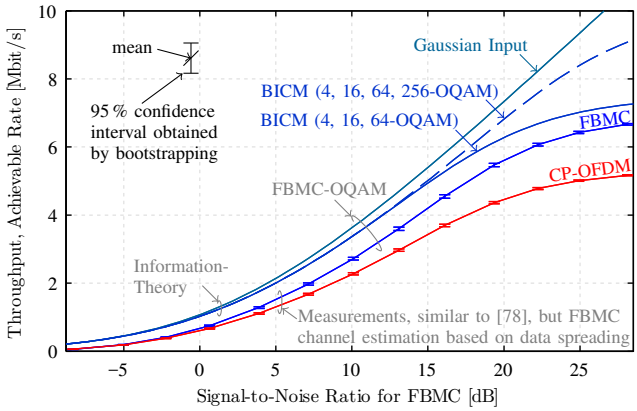


Fig. 12. **Real-world testbed measurements** at 2.5 GHz show that FBMC has a higher throughput than OFDM (1.4 MHz LTE resembling SISO signal) due to a higher available bandwidth and no CP overhead. The channel estimation in FBMC is based on the data spreading approach [65]. The measured throughput performs close to the achievable rates, based on (45) and (46).

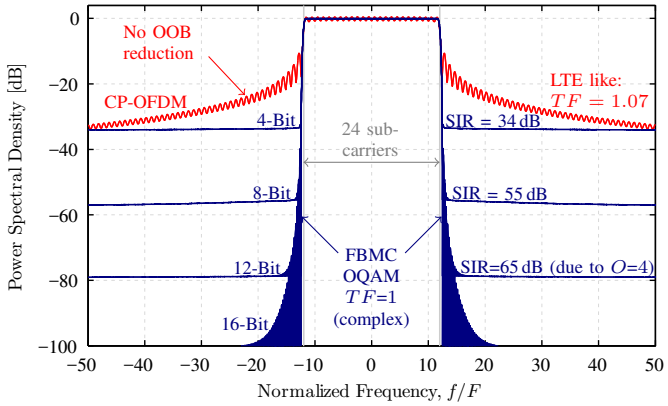


Fig. 13. The superior spectral properties of FBMC are destroyed if we include poor quality hardware. The proposed concept in Figure 1 only works if the power amplifier is sufficiently linear and the DAC resolution sufficiently high.

usable bandwidth and because no CP is used. Different to our previous paper [78] we now employ the data spreading approach discussed in Section VI-A and not auxiliary symbols. This further improves the throughput. OFDM and FBMC have the same transmit power which leads to a smaller SNR for FBMC compared to OFDM because the power is spread over a larger bandwidth [78].

The measured throughput is only 2 dB worse than the theoretical BICM bound. Such differences can be explained by an imperfect coder, a limited code length, a limited number of code rates (we employ turbo coding [79] and 15-Channel Quality Indicator (CQI) values, same as in LTE) and channel estimation errors [80]. An important observation here is that the throughput saturates. If we increase the SNR from 0 dB to 10 dB, that is, by a factor of 10, then the throughput increases by approximately 300%. On the other hand, if we increase the SNR from 20 dB to 30 dB, also a factor of 10, the throughput only increases by 20%. Even if we consider a symbol alphabet of up to 256-OQAM (BICM), the achievable rate only increases by 40%. Thus, a high SNR provides only a small throughput gain while power and hardware costs are significantly higher. We therefore often operate in medium SNR ranges.

### C. Quantization and Clipping

Figure 2 shows the superior spectral properties of FBMC compared to OFDM. Unfortunately, such figure only holds true for a sufficiently linear power amplifier and a sufficiently high DAC resolution. It was, for example, shown in [14] that nonlinearities destroy the low OOB emissions (the authors considered a highly non-linear transmission). In such cases, we might need digital predistortion which increases the computational complexity further [81]. Another aspect is the resolution of the DAC. If we employ, for example, a one-bit DAC, we essentially end up with rectangular pulses. This is exactly what we want to avoid. Figure 13 shows how the PSD depends on the resolution of the DAC ($N_{\mathrm{FFT}} = 1024$). Quantization noise leads to relatively high OOB emissions. However, all those problems are not limited to FBMC but also appear in windowed and filtered OFDM. Thus, the concept of sharp digital filters to enable a flexible time-frequency allocation, see Figure 1, only works for a sufficiently linear power amplifier and a sufficiently high DAC resolution. If these conditions are not met, we have to rely on less flexible analogue filters.

## VII. Conclusion

OFDM based schemes such as WOLA, UFMC and f-OFDM have a relatively high spectral efficiency once the number of subcarriers is high. However, not all possible use cases envisioned for future wireless systems will employ such a high number of subcarriers. For a small number of subcarriers, FBMC becomes much more efficient than OFDM, in particular if the transmission band is shared between different use cases.

Many challenges associated with FBMC, such as channel estimation and MIMO, can be efficiently dealt with, as validated by our real-world testbed measurements. Additionally, one-tap equalizers are in many practical cases sufficient once we match the subcarrier spacing (pulse shape) to the channel statistics. In highly doubly selective channels, we can switch from an FBMC-OQAM transmission to an FBMC-QAM transmission, thus deliberately sacrificing spectral efficiency but gaining robustness. This leads to an even higher SIR than in CP-OFDM.

While it is true that the computational complexity of FBMC is higher than in windowed OFDM, both methods require the same basic operations, allowing us to reuse many hardware components.

## References

[1] 3GPP, "TSG RAN; study on scenarios and requirements for next generation access technologies; (release 14)," http://www.3gpp.org/DynaReport/38913.htm, Oct. 2016.

[2] S. Schwarz and M. Rupp, "Society in motion: Challenges for LTE and beyond mobile communications," *IEEE Commun. Mag., Feature Topic: LTE Evolution*, vol. 54, no. 5, 2016.

[3] F. Schaich, T. Wild, and R. Ahmed, "Subcarrier spacing-how to make use of this degree of freedom," in *IEEE Vehicular Technology Conference (VTC Spring)*, 2016, pp. 1–6.

[4] X. Zhang, M. Jia, L. Chen, J. Ma, and J. Qiu, "Filtered-OFDM-enabler for flexible waveform in the 5th generation cellular networks," in *IEEE Global Communications Conference (GLOBECOM)*, 2015, pp. 1–6.

[5] S. Schwarz, T. Philosof, and M. Rupp, "Signal processing challenges in cellular assisted vehicular communications," *IEEE Signal Processing Magazine*, vol. 34, no. 2, pp. 47–59, March 2017.

[6] J. G. Andrews, S. Buzzi, W. Choi, S. V. Hanly, A. Lozano, A. C. Soong, and J. C. Zhang, "What will 5G be?" *IEEE Journal on Selected Areas in Communications*, vol. 32, no. 6, pp. 1065–1082, 2014.

[7] G. Wunder, P. Jung, M. Kasparick, T. Wild, F. Schaich, Y. Chen, S. Brink, I. Gaspar, N. Michailow, A. Festag *et al.*, "5GNOW: non-orthogonal, asynchronous waveforms for future mobile applications," *IEEE Communications Magazine*, vol. 52, no. 2, pp. 97–105, 2014.

[8] P. Banelli, S. Buzzi, G. Colavolpe, A. Modenini, F. Rusek, and A. Ugolini, "Modulation formats and waveforms for 5G networks: Who will be the heir of OFDM?: An overview of alternative modulation schemes for improved spectral efficiency," *IEEE Signal Process. Mag.*, vol. 31, no. 6, pp. 80–93, 2014.

[9] 3GPP, "TSG RAN; study on new radio access technology; (release 14)," http://www.3gpp.org/DynaReport/38912.htm, Sept. 2016.

[10] ——, "TSG RAN; study on new radio access technology; radio interface protocol aspects; (release 14)," http://www.3gpp.org/DynaReport/38804.htm, Mar. 2017.

[11] ——, "TSG RAN; study on new radio access technology; physical layer aspects; (release 14)," http://www.3gpp.org/DynaReport/38802.htm, Mar. 2017.

[12] M. Bellanger, D. Le Ruyet, D. Roviras, M. Terré, J. Nossek, L. Baltar, Q. Bai, D. Waldhauser, M. Renfors, T. Ihalainen *et al.*, "FBMC physical layer: a primer," *PHYDYAS, January*, 2010.

[13] B. Farhang-Boroujeny, "OFDM versus filter bank multicarrier," *IEEE Signal Processing Magazine*, vol. 28, no. 3, pp. 92–112, May 2011.

[14] A. Sahin, I. Guvenc, and H. Arslan, "A survey on multicarrier communications: Prototype filters, lattice structures, and implementation aspects," *IEEE Communications Surveys Tutorials*, vol. 16, no. 3, pp. 1312–1338, December 2012.

[15] H. Bölcskei, "Orthogonal frequency division multiplexing based on offset QAM," in *Advances in Gabor analysis*. Springer, 2003, pp. 321–352.

[16] B. Farhang-Boroujeny, "Filter bank multicarrier modulation: A waveform candidate for 5G and beyond," *Advances in Electrical Engineering*, vol. 2014, December 2014.

[17] H. Asplund, K. Larsson, and P. Okvist, "How typical is the "typical urban" channel model?" in *IEEE Vehicular Technology Conference*, 2008, pp. 340–343.

[18] L. Bernadó, T. Zemen, F. Tufvesson, A. F. Molisch, and C. F. Mecklenbräuker, "Delay and doppler spreads of nonstationary vehicular channels for safety-relevant scenarios," *IEEE Transactions on Vehicular Technology*, vol. 63, no. 1, pp. 82–93, 2014.

[19] S. Payami and F. Tufvesson, "Delay spread properties in a measured massive MIMO system at 2.6 GHz," in *IEEE International Symposium on Personal, Indoor, and Mobile Radio Communications (PIMRC)*, Sept 2013, pp. 53–57.

[20] S. Caban, J. A. García-Naya, and M. Rupp, "Measuring the physical layer performance of wireless communication systems," *IEEE Instrumentation & Measurement Magazine*, vol. 14, no. 5, pp. 8–17, 2011.

[21] M. Lerch, S. Caban, M. Mayer, and M. Rupp, "The Vienna MIMO testbed: Evaluation of future mobile communication techniques." *Intel Technology Journal*, vol. 4, pp. 58–69, 2014.

[22] R. Nissel, E. Zöchmann, M. Lerch, S. Caban, and M. Rupp, "Low-latency MISO FBMC-OQAM: It works for millimeter waves!" in *IEEE International Microwave Symposium*, Honolulu, Hawaii, June 2017.

[23] R. Nissel, M. Lerch, and M. Rupp, "Experimental validation of the OFDM bit error probability for a moving receive antenna," in *IEEE Vehicular Technology Conference (VTC)*, Vancouver, Canada, Sept 2014.

[24] E. Zöchmann, M. Lerch, S. Caban, R. Langwieser, C. Mecklenbräuker, and M. Rupp, "Directional evaluation of receive power, Rician K-factor and RMS delay spread obtained from power measurements of 60 GHz indoor channels," in *IEEE Topical Conference on Antennas and Propagation in Wireless Communications (APWC)*, 2016.

[25] M. Caus and A. I. Pérez-Neira, "Transmitter-receiver designs for highly frequency selective channels in MIMO FBMC systems," *IEEE Transactions on Signal Processing*, vol. 60, no. 12, pp. 6519–6532, 2012.

[26] L. Marijanovic, S. Schwarz, and M. Rupp, "MMSE equalization for FBMC transmission over doubly-selective channels," in *Thirteenth International Symposium on Wireless Communication Systems*, Poznan, Poland, September 2016, pp. 1–6.

[27] L. Zhang, P. Xiao, A. Zafar, R. Tafazolli *et al.*, "FBMC system: An insight into doubly dispersive channel impact," *IEEE Transactions on Vehicular Technology*, 2016, to appear.

[28] M. Fuhrwerk, J. Peissig, and M. Schellmann, "Channel adaptive pulse shaping for OQAM-OFDM systems," in *IEEE European Signal Processing Conference (EUSIPCO)*, 2014, pp. 181–185.

[29] G. Matz, D. Schafhuber, K. Grochenig, M. Hartmann, and F. Hlawatsch, "Analysis, optimization, and implementation of low-interference wireless multicarrier systems," *IEEE Transactions on Wireless Communications*, vol. 6, no. 5, pp. 1921–1931, 2007.

[30] H. G. Feichtinger and T. Strohmer, *Gabor analysis and algorithms: Theory and applications*. Springer Science & Business Media, 2012.

[31] M. Vetterli, J. Kovačević, and V. K. Goyal, *Foundations of signal processing*. Cambridge University Press, 2014.

[32] Qualcomm Incorporated, "Waveform candidates," in *3GPP TSG-RAN WG1 84b*, Busan, Korea, April 2016.

[33] F. Schaich, T. Wild, and Y. Chen, "Waveform contenders for 5G-suitability for short packet and low latency transmissions," in *IEEE Vehicular Technology Conference (VTC Spring)*, 2014, pp. 1–5.

[34] H. Nam, M. Choi, S. Han, C. Kim, S. Choi, and D. Hong, "A new filter-bank multicarrier system with two prototype filters for QAM symbols transmission and reception," *IEEE Transactions on Wireless Communications*, vol. 15, no. 9, pp. 5998–6009, 2016.

[35] Y. H. Yun, C. Kim, K. Kim, Z. Ho, B. Lee, and J.-Y. Seol, "A new waveform enabling enhanced QAM-FBMC systems," in *IEEE International Workshop on Signal Processing Advances in Wireless Communications (SPAWC)*, 2015, pp. 116–120.

[36] C. Kim, Y. H. Yun, K. Kim, and J.-Y. Seol, "Introduction to QAM-FBMC: from waveform optimization to system design," *IEEE Communications Magazine*, vol. 54, no. 11, pp. 66–73, 2016.

[37] R. Haas and J.-C. Belfiore, "A time-frequency well-localized pulse for multiple carrier transmission," *Wireless Personal Communications*, vol. 5, no. 1, pp. 1–18, 1997.

[38] R. Nissel and M. Rupp, "On pilot-symbol aided channel estimation in FBMC-OQAM," in *IEEE International Conference on Acoustics, Speech and Signal Processing (ICASSP)*, Shanghai, China, March 2016, pp. 3681–3685.

[39] M. G. Bellanger, "Specification and design of a prototype filter for filter bank based multicarrier transmission," in *IEEE International Conference on Acoustics, Speech, and Signal Processing*, vol. 4, 2001, pp. 2417–2420.

[40] S. Mirabbasi and K. Martin, "Design of prototype filter for near-perfect-reconstruction overlapped complex-modulated transmultiplexers," in *IEEE International Symposium on Circuits and Systems*, 2002.

[41] C. Lélé, P. Siohan, and R. Legouable, "The Alamouti scheme with CDMA-OFDM/OQAM," *EURASIP Journal on Advances in Signal Processing*, vol. 2010, Article ID 703513, pp. 1–13, 2010.

[42] R. Zakaria and D. Le Ruyet, "A novel filter-bank multicarrier scheme to mitigate the intrinsic interference: application to MIMO systems," *IEEE Transactions on Wireless Communications*, vol. 11, no. 3, pp. 1112–1123, 2012.

[43] R. Nissel and M. Rupp, "Bit error probability for pilot-symbol aided channel estimation in FBMC-OQAM," in *IEEE International Conference on Communications (ICC)*, Kuala Lumpur, Malaysia, May 2016.

[44] G. Matz, H. Bolcskei, and F. Hlawatsch, "Time-frequency foundations of communications: Concepts and tools," *IEEE Signal Processing Magazine*, vol. 30, no. 6, pp. 87–96, 2013.

[45] C. Lélé, P. Siohan, R. Legouable, and M. Bellanger, "CDMA transmission with complex OFDM/OQAM," *EURASIP Journal on Wireless Communications and Networking*, vol. 2008, Article ID 748063, pp. 1–12, 2008.

[46] R. Nissel and M. Rupp, "Enabling low-complexity MIMO in FBMC-OQAM," in *IEEE Globecom Workshops (GC Wkshps)*, Washington DC, USA, Dec 2016.

[47] ——, "OFDM and FBMC-OQAM in doubly-selective channels: Calculating the bit error probability," *IEEE Communications Letters*, 2017, to appear.

[48] D. S. Waldhauser, L. G. Baltar, and J. A. Nossek, "MMSE subcarrier equalization for filter bank based multicarrier systems," in *IEEE Workshop on Signal Processing Advances in Wireless Communications*, 2008, pp. 525–529.

[49] P. Siohan, C. Siclet, and N. Lacaille, "Analysis and design of OFDM/OQAM systems based on filterbank theory," *IEEE Transactions on Signal Processing*, vol. 50, no. 5, pp. 1170–1183, 2002.

[50] M. Terre, "FBMC modulation / demodulation," Matlab Central: https://www.mathworks.com/matlabcentral/.

[51] ITU, "Recommendation ITU-R M.1225: Guidelines for Evaluation of Radio Transmission Technologies for IMT-2000," ITU, Tech. Rep., 1997.

[52] F.-M. Han and X.-D. Zhang, "Wireless multicarrier digital transmission via Weyl-Heisenberg frames over time-frequency dispersive channels," *IEEE Transactions on Communications*, vol. 57, no. 6, 2009.
[53] P. Robertson and S. Kaiser, "The effects of Doppler spreads in OFDM(A) mobile radio systems," in *IEEE Vehicular Technology Conference (VTC Fall)*, 1999, pp. 329–333.
[54] 3GPP, "TSG RAN; study on channel model for frequency spectrum above 6GHz; (release 14)," http://www.3gpp.org/DynaReport/38900.htm, Dec. 2016.
[55] M. Fuhrwerk, J. Peissig, and M. Schellmann, "On the design of an FBMC based air interface enabling channel adaptive pulse shaping per sub-band," in *IEEE Signal Processing Conference (EUSIPCO)*, 2015, pp. 384–388.
[56] Q. Bodinier, F. Bader, and J. Palicot, "Coexistence in 5G: Analysis of cross-interference between OFDM/OQAM and legacy users," in *IEEE Globecom Workshops (GC Wkshps)*, 2016.
[57] C. Thein, M. Fuhrwerk, and J. Peissig, "About the use of different processing domains for synchronization in non-contiguous FBMC systems," in *IEEE International Symposium on Personal, Indoor, and Mobile Radio Communications (PIMRC)*, Sept 2013, pp. 791–795.
[58] G. P. Fettweis, "The tactile internet: Applications and challenges," *IEEE Vehicular Technology Magazine*, vol. 9, no. 1, pp. 64–70, 2014.
[59] C. Lélé, J.-P. Javaudin, R. Legouable, A. Skrzypczak, and P. Siohan, "Channel estimation methods for preamble-based OFDM/OQAM modulations," *European Transactions on Telecommunications*, vol. 19, no. 7, pp. 741–750, 2008.
[60] D. Katselis, E. Kofidis, A. Rontogiannis, and S. Theodoridis, "Preamble-based channel estimation for CP-OFDM and OFDM/OQAM systems: A comparative study," *IEEE Trans. Signal Process.*, vol. 58, no. 5, pp. 2911–2916, 2010.
[61] E. Kofidis, D. Katselis, A. Rontogiannis, and S. Theodoridis, "Preamble-based channel estimation in OFDM/OQAM systems: a review," *Signal Processing*, vol. 93, no. 7, pp. 2038–2054, 2013.
[62] D. Kong, D. Qu, and T. Jiang, "Time domain channel estimation for OQAM-OFDM systems: algorithms and performance bounds," *IEEE Transactions on Signal Processing*, vol. 62, no. 2, pp. 322–330, 2014.
[63] J.-P. Javaudin, D. Lacroix, and A. Rouxel, "Pilot-aided channel estimation for OFDM/OQAM," in *IEEE Vehicular Technology Conference (VTC)*, vol. 3, 2003, pp. 1581–1585.
[64] T. H. Stitz, T. Ihalainen, A. Viholainen, and M. Renfors, "Pilot-based synchronization and equalization in filter bank multicarrier communications," *EURASIP Journal on Advances in Signal Processing*, vol. 2010, p. 9, 2010.
[65] C. Lélé, R. Legouable, and P. Siohan, "Channel estimation with scattered pilots in OFDM/OQAM," in *IEEE Workshop on Signal Processing Advances in Wireless Communications (SPAWC)*, 2008, pp. 286–290.
[66] B. Yu, S. Hu, P. Sun, S. Chai, C. Qian, and C. Sun, "Channel estimation using dual-dependent pilots in FBMC/OQAM systems," *IEEE Communications Letters*, vol. 20, no. 11, pp. 2157–2160, Nov 2016.
[67] J.-M. Choi, Y. Oh, H. Lee, and J.-S. Seo, "Interference-dependent pair of pilots for channel estimation in FBMC systems," in *IEEE International Symposium on Broadband Multimedia Systems and Broadcasting*, 2016, pp. 1–4.
[68] C. Lélé, "Iterative scattered-based channel estimation method for OFDM/OQAM," *EURASIP Journal on Advances in Signal Processing*, vol. 2012, no. 1, p. 42, 2012.
[69] J. Bazzi, P. Weitkemper, and K. Kusume, "Power efficient scattered pilot channel estimation for FBMC/OQAM," in *International ITG Conference on Systems, Communications and Coding*. VDE, 2015, pp. 1–6.
[70] W. Cui, D. Qu, T. Jiang, and B. Farhang-Boroujeny, "Coded auxiliary pilots for channel estimation in FBMC-OQAM systems," *IEEE Transactions on Vehicular Technology*, vol. 65, no. 5, pp. 2936–2946, May 2016.
[71] R. Nissel, E. Zöchmann, and M. Rupp, "On the influence of doubly-selectivity in pilot-aided channel estimation for FBMC-OQAM," in *IEEE Vehicular Technology Conference (VTC Spring)*, 2017, pp. 1–5.
[72] M. Fuhrwerk, S. Moghaddamnia, and J. Peissig, "Scattered pilot-based channel estimation for channel adaptive FBMC-OQAM systems," *IEEE Transactions on Wireless Communications*, vol. 16, no. 3, pp. 1687–1702, March 2017.
[73] D. Tse and P. Viswanath, *Fundamentals of wireless communication*. Cambridge university press, 2005.
[74] G. Caire, G. Taricco, and E. Biglieri, "Bit-interleaved coded modulation," *IEEE Transactions on Information Theory*, vol. 44, no. 3, pp. 927–946, 1998.
[75] A. G. i Fàbregas, A. Martinez, and G. Caire, *Bit-interleaved coded modulation*. Now Publishers Inc, 2008.
[76] R. Nissel, S. Caban, and M. Rupp, "Closed-Form capacity expression for low complexity BICM with uniform inputs," in *IEEE International Symposium on Personal, Indoor and Mobile Radio Communications (PIMRC)*, Hong Kong, P.R. China, Aug. 2015, pp. 678–682.
[77] C. Novak and G. Matz, "Low-complexity MIMO-BICM receivers with imperfect channel state information: Capacity-based performance comparison," in *IEEE Workshop on Signal Processing Advances in Wireless Communications (SPAWC)*, Marrakech, Morocco, June 2010.
[78] R. Nissel, S. Caban, and M. Rupp, "Experimental evaluation of FBMC-OQAM channel estimation based on multiple auxiliary symbols," in *IEEE Sensor Array and Multichannel Signal Processing Workshop (SAM)*, Rio de Janeiro, Brazil, July 2016.
[79] H. Zarrinkoub, *Understanding LTE with MATLAB: from mathematical modeling to simulation and prototyping*. John Wiley & Sons, 2014.
[80] S. Schwarz, M. Simko, and M. Rupp, "On performance bounds for MIMO OFDM based wireless communication systems," in *Signal Processing Advances in Wireless Communications SPAWC 2011*, San Francisco, CA, June 2011, pp. 311 –315.
[81] T. Gotthans, R. Maršálek, J. Blumenstein, and G. Baudoin, "Experimental evaluation of digital predistortion with FBMC and OFDM signals," in *IEEE Annual Wireless and Microwave Technology Conference (WAMICON)*, April 2015, pp. 1–3.